CERAMIC PROCESSING ROUTE AND CHARACTERIZATION OF A Ni-Zn FERRITE FOR APPLICATION IN A PULSED-CURRENT MONITOR

V. L. O. Brito and A. C. C. Migliano

Instituto de Estudos Avançados
Divisão de Física Aplicada
Rodovia dos Tamoios, km 5,5, São José dos Campos
SP 12228-001, Brazil

L. V. Lemos

Instituto Tecnológico de Aeronáutica
Programa de Pós-Graduação em Engenharia Aeronáutica e Mecânica
Praça Marechal Eduardo Gomes, 50, São José dos Campos
SP 12228-900, Brazil

F. C. L. Melo

Instituto de Aeronáutica e Espaço
Divisão de Materiais
Praça Marechal Eduardo Gomes, 50, São José dos Campos
SP 12228-900, Brazil

Abstract—Pulsed-current sensors require transducers constituted of magnetic materials with high magnetic permeability in a frequency range compatible with the period and the frequency of the current pulse. The use of ferrites in this application has the advantage of low cost and low losses in high frequencies. The aim of this work is to present a procedure for selection of the ceramic processing route of Ni-Zn ferrite for application in a pulsed-current sensor. The ferrite samples were prepared under different processing parameters and characterized in terms of microstructure, chemical analysis, complex magnetic permeability, and magnetic hysteresis. The chosen processing route included high energy milling of the pre-sintered powder, its disaggregation before sample forming, and sintering of the samples

Corresponding author: V. L. O. Brito (vlobrito@ieav.cta.br).

in air for 2 h at 1300°C. Tests were performed and it was verified that using this processing route for the fabrication of the sensor's core it was possible to monitor pulses of 0.1–1.0 μs.

1. INTRODUCTION

Ni-Zn ferrites are spinel ferrimagnetic ceramics, generally represented by $Ni_{1-x}Zn_xFe_2O_4$. The magnetic properties of these materials are very sensitive to variations in chemical composition and microstructure [1]. The high electric resistivity of these materials provides low eddy-current losses, which is desirable for a ferrimagnetic core. Besides, the fabrication of ceramic cores is relatively simple and may be carried out by means of conventional ceramic methods. The sintering of Ni-Zn ferrites is simpler than the sintering of other high permeability ferrites, such as the Mn-Zn ones, because controlled atmosphere is not necessarily required [2].

Figure 1 [3] shows a *pulsed-current monitor* (PCM) containing a toroidal Ni-Zn ferrite core. The pulsed electron beam passes through the aperture and the magnetic field associated to the beam causes a magnetic induction (B) in the core. The ceramic isolator, fixed by means of a metal-ceramic weld, eliminates the effect of reverse currents in the metallic structure of the device.

The current sensor works as a current transformer, in which the primary is either a conductor or an electron beam, treated as a one-turn coil with infinite radius. The secondary is the coil around the
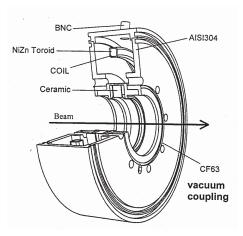

Figure 1. CF63-type pulse transformer used in vacuum lines [3].

core, having N turns. The current from the secondary passes through an integrating circuit and the voltage at the output of the PCM may be monitored by means of an oscilloscope. The output voltage in the secondary terminal, V, is proportional to the magnetic permeability, μ_r, of the core (1):

$$V \propto \frac{NA\mu_r}{r}\frac{di}{dt},\tag{1}$$

where A is the cross-sectional area of the core, r is the mean radius of the toroidal core, and di/dt is the current variation with time. If the magnetic permeability of the core is too low, the sensitivity of the current monitor will be impaired.

The core's saturation induction (B_s) is also an important parameter, since the current monitor has to be designed in a way that the magnetic field associated to the pulsed current does not saturate the core. In spite of the relatively low saturation induction, ferrites have low coercivity and low hysteresis losses, when compared to other metallic materials used as magnetic cores [4]. A capacitor and a resistor incorporated in the secondary circuit compose the shunt circuit, i.e., the pulse former circuit.

The aim to obtain a high sensitivity current sensor leads to the choice of a core material with highest magnetic permeability. The $Ni_{1-x}Zn_xFe_2O_4$ ferrites with $x \approx 0.7$ usually presents the highest levels of magnetic permeability of Ni-Zn ferrites but only in frequencies lower than approximately 200 kHz [5]. Other limitations of this composition are:

- Relatively low Curie temperature ($\approx 77°C$) and high variation of the magnetic permeability with temperature [6];

- The variation of the magnetic permeability with Zn fraction is increased when x approximates 0.7 [1, 7]. Thus, small heterogeneities in the chemical composition of the batch may result in ferrite pieces with different magnetic properties;

- The magnetic permeability of the ferrite with $x = 0.7$ varies much more with sintering temperature than do ferrites with lower x values [5]. Thus, the sintering temperature must be more carefully controlled in this case.

For application in a PCM for 1 µs pulse duration, it is required that the magnetic permeability of the ferrite be high and approximately constant with frequency for frequencies up to 1 MHz at least. Literature [5] has shown that $Ni_{0.5}Zn_{0.5}Fe_2O_4$ attends this requirement, with a Curie temperature near 230°C and a saturation induction [8] attaining 90 mT. It is possible to optimize the magnetic properties of Ni-Zn ferrites by means of a proper adjustment of the sintering

conditions and the use of sintering additives [9–11]. Stoppels [12] mentioned that CaO, SiO, TiO_2, Nb_2O_5, Ta_2O_5, V_2O_5, and HfO_2 additions increase the resistivity of ferrites (acting either at grain boundaries or inside the grains), consequently reducing the eddy current losses. According to the author, literature had shown that a 200 ppm Nb_2O_5 addition apparently suppresses zinc evaporation in grain boundaries during sintering, reducing internal stresses.

The aim of this work is to show a procedure for adjusting the processing route and characterization of a Ni-Zn ferrite for application in PCM for pulses shorter than 1 μs.

2. EXPERIMENTAL PROCEDURE

2.1. Ceramic Cores

The raw materials for fabrication of the ferrite were weighed in the proportion (mol%): 25.5%NiO-26.1%ZnO-48.4%Fe_2O_3. The raw materials were wet-mixed in a ball mill, using an alumina jar.

After dried in a furnace, the mixed material was uniaxially compacted in 37-mm diameter tablets and pre-sintered at 900°C for 2 h. The aim of the compaction was to enhance the pre-sintering process. The tablets were manually broken and subsequently triturated in a pulverizer. The triturated powder was sieved to 115 mesh and uniaxially compacted in round tablets at 50 MPa (samples for microstructural observation) and cylinders (samples for magnetic characterization). 0.6 weight% of carboxymethylcellulose (CMC) was added to the powder before compacting the cylinders: The CMC was dissolved in distilled water and the powder was added to the solution. The water in excess was dried in a furnace and the slightly humid powder was forced against a nylon sieve, simulating pelletization.

Samples were sintered at 1200°C, 1300°C, and 1400°C for 2 h in air. For magnetic characterization, three samples were sintered in each temperature. Powder portions were also sintered at those temperatures and subsequently underwent chemical analysis by means of atomic absorption spectroscopy.

The samples for microstructural observation were polished and etched. Grain size measurements and quantitative analysis were carried out based on the ASTM E112 standard [13].

After measuring the complex magnetic permeability, described in the next section, it was verified which sintering temperature was the most suitable one for the purpose of this work. Another batch was prepared, following the same procedure, until pulverization. The pre-sintered powder was dry-milled in a Spex high-energy mill for 2 h. The

powder's particle size was evaluated by means of scanning electron microscopy (SEM).

The milled powder was prepared for sample formation, under the following conditions:

- Condition 1: Same procedure as the first batch;
- Condition 2: 200 ppm Nb_2O_5 was added to the powder. The powder was mixed in acetone with a glass stick and simultaneously disaggregated in ultrasonic bath for 15 minutes. The powder was subsequently dried in a furnace and the CMC addition was carried out, as done in Condition 1;
- Condition 3: The powder was disaggregated in acetone, with ultrasonic bath for 15 minutes, and dried in a furnace. CMC addition was subsequently carried out, as done in Condition 1.

The samples were sintered in the selected sintering temperature, for 2 h in air. The complex magnetic permeability was measured. Comparing the results from Condition 1 to those of Condition 3, one can verify the influence of the disaggregation step on the properties of the ferrite. Comparing Condition 2 to Condition 3, one can verify the influence of the Nb_2O_5 addition. The most suitable condition was selected and the following characterization was carried out: Analysis of the complex magnetic permeability under temperature variation and determination of the saturation induction (B_s), both detailed in the next section.

Samples from all routes tested in this work underwent the following characterization:

- Density analysis by means of the Archimedes method;
- X-ray diffraction analysis with Cu Kα radiation.

2.2. Core's Magnetic Characterization

The relative complex magnetic permeability of the samples were measured, in the 100 kHz–100 MHz frequency range, using an Agilent 4194 A impedance analyzer and a one-port measuring method, according to [14]. The real (μ_r') and imaginary (μ_r'') parts of the relative complex magnetic permeability were automatically calculated from the resistance and reactance values measured, using expressions:

$$\mu_r' = \frac{c}{\omega d}\left(\frac{X_{in}^{short}}{Z_0^{air}}\right) \tag{2}$$

$$\mu_r'' = \frac{c}{\omega d}\left(\frac{R_{in}^{short}}{Z_0^{air}}\right) \tag{3}$$

$$Z_0^{air} = 138\log\left(\frac{D_e}{D_i}\right) \tag{4}$$

where c is the speed of light, ω is the angular frequency, and d is the length of the tubular sample. Z_0^{air} is the characteristic impedance of the circuit filled with air. $X_{\text{in}}^{\text{short}}$ is the reactance of the circuit, measured with the sample placed inside the sample-holder. $R_{\text{in}}^{\text{short}}$ is the resistance of the circuit, also measured with the sample placed inside the sample-holder. D_e and D_i are the external and internal diameters of the sample. Observe in (4) that corrections were considered in order to take into account the air gap in the coaxial-line sample holder.

The cylindrical ferrite samples for complex magnetic permeability characterization were machined, either in their internal or external diameters, in order to fit the coaxial sample-holder, which allowed samples with $D_e < 7.0\,\text{mm}$ and $D_i > 3.05\,\text{mm}$. The lengths of the samples were between 4.345 mm and 9.065 mm. All samples had their internal and external diameter surfaces painted with silver paint before measuring. The complex magnetic permeability under temperature variation was measured between $-40°\text{C}$ and $+50°\text{C}$. The sample holder was placed inside an ESPEC SH-241 chamber, varying temperature in steps of $10°\text{C}$, and remaining for 15 minutes at each test temperature. The B_s parameter was obtained from hysteresis curves. The three tubular samples fabricated for this characterization had $D_e \approx 7.36\,\text{mm}$, $D_i \approx 4.27\,\text{mm}$, and d between 2.75 mm and 2.89 mm. A BRASMAG BM 250-A hysteresis curve tracer and an oscilloscope were used in this test.

2.3. PCM Assembly and Characterization

A PCM was assembled, employing a circuit constituted by:

- A toroidal inductor with ferrite core ($D_e = 7.3\,\text{mm}$; $D_i = 4.4\,\text{mm}$; $d = 2.6\,\text{mm}$) and 20 turns with 8 AWG copper wire;
- Low-pass circuit, operating as the pulse former circuit, constituted of a 262,5 pF capacitor and a 50 Ω resistor.

The calibration of the PCM was carried out using the following apparatus: Agilent's 81101 A pulse generator, 50 Ω shunt resistance, and Tektronix's TDS 540 A oscilloscope.

3. RESULTS AND DISCUSSION

3.1. Characterization of the Ferrite Core

Figure 2 shows the microstructures of the ferrites and Table 1 shows data on the grain size distribution. The densities of the tubular samples sintered at $1200°\text{C}$, $1300°\text{C}$, and $1400°\text{C}$ were, respectively,
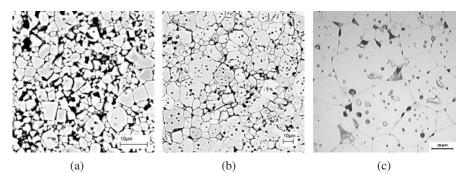
(a)   (b)   (c)

Figure 2. Microstructure of the ferrite samples sintered at (a) 1200°C, (b) 1300°C, and (c) 1400°C.

Table 1. Grain size distribution of the sintered ferrite samples.

Sintering temperature	Average (μm)	Mode (μm)	Std. Dev. (μm)	% RA*
1200°C	1.8	1.3	1.1	8.3
1300°C	7.9	5.9	5.2	9.6
1400°C	23.2	7.3	14.2	8.1

*Percent relative accuracy.

4.75, 4.71, and 4.93 g/cm^3. The porosity of the sample sintered at 1200°C is predominately intergranular, whereas the porosity of the samples sintered at 1300°C and 1400°C is located at grain boundaries and inside the grains.

Figure 3 shows the results of complex magnetic permeability of all ferrite samples fabricated from the first batch. One can notice that the sintering temperature of 1200°C resulted in a material applicable in higher frequencies, but the level attained by the magnetic permeability makes it less sensitive to the magnetic field associated to the pulsed current to be monitored. The losses (μ_r'') obtained with sintering at 1200°C are lower due to the microstructure of the material, constituted of smaller grains. It is well known that the presence of high resistitvity regions in the microstrucure, such as grain boundaries, reduces losses in higher frequencies, increasing the μ_r' values. On the other hand, it isn't possible to obtain the highest μ_r' levels of the ferrite with smaller grains. Literature [15] has mentioned that the magnetic permeability of Ni-Zn ferrites usually increases linearly with grain size until $\approx 5\,\mu$m. For larger grain sizes, permeability increases in a lower rate or even decreases.
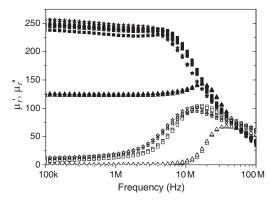
Figure 3. Complex magnetic permeability of the ferrite samples. Solid: μ_r'; hollow: μ_r'', $1200°C$ ($\blacktriangle, \triangle$); $1300°C$ ($\blacksquare, \square$); $1400°C$ ($\bigstar, \star$).

Table 2. Average magnetic properties at 1 MHz.

Sintering temperature	μ_r'	Loss factor (%)
1200°C	124	0.3
1300°C	236	5.4
1400°C	243	7.6

Table 2 shows the μ_r' values at 1 MHz and the loss factors (which correspond to μ_r''/μ_r') at this frequency. This frequency was chosen because it corresponds to a 1 µs period, which is within the range aimed in this work. It is observed that the sintering temperature of 1400°C raised the average value of μ_r' in 3% when compared to the results obtained with sintering at 1300°C but the loss factor increased in 41%. Thus, it was decided that the 1300°C sintering temperature provided the most suited complex magnetic permeability to the ferrite for the proposed application.

Figure 4 shows the diffractograms of the ferrites obtained, presenting typical spinel crystal structure and no evidence of second phases.

Table 3 shows the results of chemical analysis. The oxygen percentages were estimated as being the remaining to complete 100% and the results obtained for sintering at 1200°C and 1300°C were lower than the expected. It has been reported [16] that a sintering atmosphere in which the partial pressure of oxygen is too low may induce oxygen vacancies in the ferrite, as a consequence of the reduction
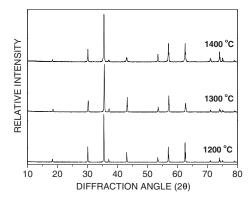
Figure 4. Diffractograms of the ferrites sintered at different temperatures.

Table 3. Results (in mass%) from chemical analysis of the ferrite in the pre-sintered state and after sintering at different temperatures.

Element	Pre-sintered	$1200°C$	$1300°C$	$1400°C$
Fe	46.02	47.21	51.52	48.11
	(±0.69)	(±0.96)	(±0.81)	(±0.96)
Ni	10.51	11.50	9.38	11.42
	(±0.18)	(±1.19)	(±0.25)	(±1.15)
Zn	13.84	15.60	13.92	13.56
	(±0.71)	(±1.03)	(±0.26)	(±1.01)
O	29.63*	25.69*	25.18*	26.91*

*Estimated.

of Fe. This phenomenon may impair the densification process. It also must be taken into account that the estimated oxygen fractions incorporated the errors of the measures of Fe, Ni, and Zn.

Figure 5 shows a SEM micrograph of the pre-sintered powder after milling in the high-energy mill. One can observe the presence of particles smaller than 200 nm and some agglomerates.

Figure 6 shows the diffractograms of the ferrite samples obtained from the second batch. One can notice that no second phases were detected. In this batch, the Nb_2O_5 addition wasn't expected to be detected by x-ray diffraction because the amount of additive was too small.

The densities of the tubular samples obtained from Conditions 1, 2, and 3 were, respectively, 4.56, 4.62, and 4.68 g/cm³. These values are
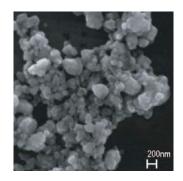
Figure 5.   SEM micrograph of the pre-sintered powder that constituted the samples of the second batch.
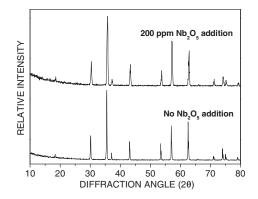

Figure 6. Diffractograms of the ferrite samples of the second batch.

lower than the ones obtained in the first batch because the latter were formed from a powder constituted of fine particles and agglomerates. The packing of a powder with such characteristic is more difficult, sometimes leading to lower density.

Figure 7 shows the complex magnetic permeability of the ferrites obtained from the second batch. The results presented very low scattering. As expected, the increase of μ'_r levels of the ferrite is obtained to the detriment of high frequency permeability [17]. The Nb_2O_5 addition reduced the low frequency μ'_r in 20 or so. The reduction of μ'_r as a result of Nb_2O_5 addition has been reported in literature, for additions higher than the one used here [14, 15]. In the work from Parvatheeswara Rao et al. [18], both μ'_r and μ''_r of a $Ni_{0.35}Zn_{0.65}Fe_2O_4$ ferrite were slightly reduced with the increase of the Nb_2O_5 addition from 0.3 wt% to 1.5 wt%. Besides the eddy
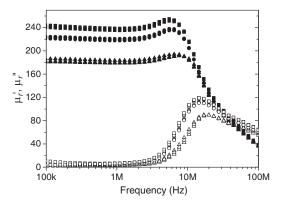
Figure 7. Complex magnetic permeability of the ferrites obtained from the second batch. Solid: μ'_r; hollow: μ''_r, Condition 1 ($\blacktriangle, \triangle$); Condition 2 ($\bullet, \circ$); Condition 3 ($\blacksquare, \square$).

Table 4. Complex magnetic permeability results at 1 MHz.

Condition	μ'_r	Loss factor (%)
1	181	1.7
2	219	2.1
3	237	2.6

current reduction, the literature [19, 20] has mentioned that Nb_2O_5 may significantly reduce the residual losses at high frequencies. One can observe here that even very low Nb_2O_5 additions may affect the μ'_r of the ferrite.

Table 4 shows the complex magnetic permeability values at 1 MHz. Comparing Condition 2 to Condition 3, one can observe that the loss ratio was reduced, but very slightly, when Nb_2O_5 was added to the ferrite. It leads one to suspect that the disaggregation step contributed more to affect the losses of the samples from Condition 2 than did the Nb_2O_5 addition. The loss ratio of Condition 1 is the lowest, due to the lower density of the samples. This happens because pores are insulating and contribute to the lowering of eddy current losses.

Based on the complex magnetic permeability results obtained, it was verified that Condition 3 provided the most suited properties for application in the current monitor proposed.

Figure 8 shows the complex magnetic permeability, under temperature variation, of a sample from Condition 3. At 1 MHz, μ'_r varies from 163 to 271 and μ''_r is practically temperature independent,
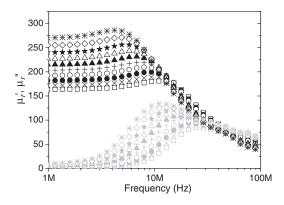
Figure 8. Complex magnetic permeability of the ferrite (Condition 3) at different temperatures: $-40°$C ($\square$); $-30°$C ($\times$); $-20°$C ($\bullet$); $-10°$C ($\circ$); $0°$C ($+$); $+10°$C ($\blacktriangle$); $+20°$C ($\triangle$); $+30°$C ($\star$); $+40°$C ($\lozenge$); $+50°$C ($\ast$). Black: μ_r'; grey: μ_r''.
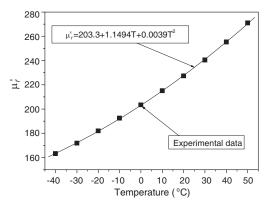

Figure 9. Real part of the complex magnetic permeability, as a function of temperature, at 1 MHz.

making the loss factor decrease when temperature increases.

Figure 9 shows the variation of μ_r' with temperature at 1 MHz. Such figure also shows the expression of the second-degree polynomial obtained after fitting of the experimental data. This information may be used for compensation of the inductance variation of the transducer with temperature. Cedillo et al. [21], testing a similar Ni-Zn ferrite, verified that the more homogeneous the chemical composition of the ferrite, the larger the μ_r' variation rate with temperature. In their work, they established a relationship between sintering conditions and
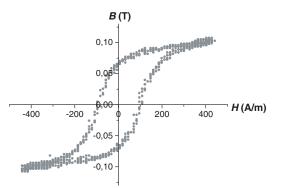
Figure 10. Hysteresis curve of sample 3.

Table 5. Data extracted from hysteresis curves of three ferrite samples.

Sample	B_s (mT)	H (A/m)
1	98	278
2	74	256
3	93	297
Average	88	277

chemical homogeneity of the ferrite.

In order to determine the maximum intensity of the current to be monitored, the saturation induction of the ferrite must be evaluated. Table 5 contains data (saturation induction (B_s) and the field intensity (H) causing saturation) extracted from hysteresis curves of three samples of the ferrite. Figure 10 shows the hysteresis curve of sample 3.

From Table 5, one can verify that the minimum magnetic field necessary to saturate the ferrite core was 256 A/m, with $B_s = 74$ mT. These results corroborate the data found on literature [8, 22] that report B_s values varying from 36 to 94 mT for similar ferrites.

3.2. PCM Characterization

The average sensitivity of the PCM was (2.43 ± 0.02) V/A, linear, for a 20–200 mA range. The device was capable of reproducing pulses with 0.10–1.0 µs, with a damping rate of less than 155.5% per µs, and amplitude of about 4.7 A. The rise and fall times of the original pulses studied were between 5 and 50% of the total pulse width and the pulses reproduced by the PCM presented a 6% delay.
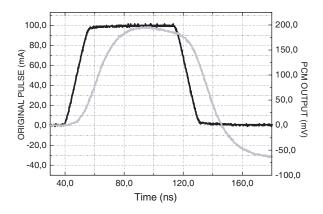
Figure 11. Representation of a 100 mA/150 ns current pulse. Black: Original pulse; grey: PCM output.

Figure 11 shows the features of a 100 mA/150 ns pulse reproduced by the PCM. One can observe that for a pulse width equivalent to a 10 MHz frequency, frequency in which μ'_r of the ferrite core is descending, the device is still capable of sensing the current pulse. Also, the quality of the output signal may be further improved by adjusting the core size, changing and/or adding new components to the pulse former circuit.

4. CONCLUSION

Ni-Zn ferrite samples were fabricated by different processing routes in order to obtain a material for application in a pulsed-current sensor, for monitoring pulses of 1 μs width or shorter. It was verified that the most suitable processing route was: Wet mixing of oxides for 8 h-drying — compaction of the mixture — pre-sintering at 900°C for 2 h-grinding — high-energy milling for 2 h-powder disaggregation in ultrasonic bath-sample formation — sintering at 1300°C for 2 h. At 1 MHz, the magnetic properties of the samples obtained by such route were: $\mu'_r = 203.2 + 1.1494\,\mathrm{T} + 0.0039\,\mathrm{T}^2$ (for $-40°\mathrm{C} < \mathrm{T} < +50°\mathrm{C}$) and minimum saturation induction of 74 mT (for a 256 A/m field). Tests were performed and it was verified that using this material in the sensor's core, it was possible to monitor current pulses between of 0.1–1 μs width.

REFERENCES

1. Brito, V. L. O., "Seleção, elaboração e caracterização de ferritas Ni-Zn para aplicação em monitores de corrente pulsada," Ph.D. Thesis, 75, Instituto Tecnológico de Aeronáutica, 2007.

2. Goldman, A., *Modern Ferrite Technology*, 2nd edition, 184, Springer, New York, 2006.

3. De Polli, Y. C., A. C. C. Migliano, C. R. S. Stopa, S. I. Nabeta, and J. R. Cardoso, "Finite element analysis of impedance of an electron beam current monitor," *IEEE Trans. Magn.*, Vol. 35, No. 3, 1833–1836, 1999.

4. McLyman, T., *Magnetic Core Selection for Transformers and Inductors*, 155, 2nd Edition, Marcel Dekker Inc., New York, 1997.

5. Smit, J. and H. P. J. Wijn, *Ferrites*, Philip's Technical Library, 1959.

6. Valenzuela, R., *Magnetic Ceramics*, Cambridge University Press, 1994.

7. Brito, V. L. O., F. C. L. Melo, and A. C. C. Migliano, "Microstructure and complex magnetic permeability of $Ni_{0.3}Zn_{0.7}Fe_2O_4$ ferrite," *Mater. Sci. Forum*, Vols. 591–593, 125–129, 2008.

8. Das, A. R., V. S. Ananthan, and D. C. Khan, "Lattice parameter variation and magnetization studies and titanium-, zirconium-, and tin-substituted nickel-zinc ferrites," *J. Appl. Phys.*, Vol. 57, No. 1, 4189–4191, 1985.

9. Rezlescu, E., L. Sachelarie, P. D. Popa, and N. Rezlescu, "Effect of substitution of divalent ions on the electrical and magnetic properties of Ni-Zn-Me ferrites," *IEEE Trans. Magn.*, Vol. 36, No. 6, 3962–3967, 2000.

10. Mirzaee, O., M. A. Golozar, and A. Shafyei, "Influence of V_2O_5 as an effective dopant on the microstructure development and magnetic properties of $Ni_{0.64}Zn_{0.36}Fe_2O_4$," *Mater. Charact.*, Vol. 59, 638–641, 2008.

11. Mangalaraja, R. V., S. T. Lee, S. Ananthakumar, P. Manohar, and C. P. Camurri, "Effect of composition on initial permeability of $Ni_{1-x}Zn_xFe_2O_4$ prepared by flash combustion technique," *Mater. Sci. Eng. A.*, Vol. 476, 234–239, 2008.

12. Stoppels, D., "Developments in soft magnetic power ferrites," *J. Magn. Magn. Mater.*, Vol. 160, 323–328, 1996.

13. *E112-96: Standard Test Methods for Determining Average Grain Size*, ASTM International, West Conshohoken, 2004.

14. Côrtes, A. L., A. C. C. Migliano, V. L. O. Brito, and

A. J. F. Orlando, "Practical aspects of the characterization of ferrite absorber using one-port device at RF frequencies," *Progress In Electromagnetics Research Symposium Proceedings*, Massachusetts Institute of Technology, Cambridge, 683–687, 2007.

15. Globus, A. and R. V. Monjaras, "Influence of the deviation from stoichiometry on the magnetic properties of Zn-rich NiZn ferrites," *IEEE Trans. Magn.*, Vol. 11, No. 5, 1300–1302, 1975.

16. Zhiyuan, L., X. Maoren, and Z. Qingqiu, "Effects of iron deficiency on magnetic properties of $(Ni_{0.76}Zn_{0.24})O(Fe_2O_3)_{0.575}$ ferrite," *J. Magn. Magn. Mater.*, Vol. 219, 9–14, 2000.

17. Visser, E. G. and M. T. Johnson, "A novel interpretation of the complex permeability in polycrystalline ferrites," *J. Magn. Magn. Mater.*, Vol. 101, 143–147, 1991.

18. Parvatheeswara Rao, B., O. Caltun, I. Dumitru, and L. Spinu, "Complex permeability spectra of Ni-Zn ferrites doped with V_2O_5/Nb_2O_5," *J. Magn. Magn. Mater.*, Vol. 304, e749–e751, 2006.

19. Kim, H. T. and H. B. Im, "Effects of Bi_2O_3 and Nb_2O_5 on the magnetic properties of Ni-Zn ferrites and lithium ferrites," *IEEE Trans. Magn.*, Vol. 18, 1541–1543, 1982.

20. Inaba, H., T. Abe, Y. Kitano, and J. Shimomura, "Magnetic properties and the grain boundary structure of Mn-Zn ferrites with the addition of Nb_2O_5," *J. Magn. Magn. Mater.*, Vol. 133, 487–489, 1994.

21. Cedillo, E., J. Ocampo, V. Rivera, and R. Valenzuela, "An apparatus for the measurement of initial magnetic permeability as a function of temperature," *J. Phys. E: Scientific Instruments*, Vol. 13, 383, 1980.

22. Khedr, M. H., A. A. Omar, M. I. Nasr, and E. K. Sedeek, "Effect of firing temperature on microstructure and magnetic properties of nanocrystalline $Ni_{0.5}Zn_{0.5}Fe_2O_4$ prepared by wet and dry methods," *J. Anal. Appl. Pyrolysis*, Vol. 76, 203–208, 2006.